Oxygen-Induced Degradation in C_{60} Based Organic Solar Cells: Relation Between Film Properties and Device Performance

João P. Bastos†‡, Eszter Voroshazi†, Eduard Fron§, Guy Brammertz†, Tim Vangerven¦, Mark Van der Auweraer§, Jef Poortmans†‡, David Cheyns †*

† - imec, Kapeldreef 75, B-3001, Leuven, Belgium

‡ - ESAT, Katholieke Universiteit Leuven, Kasteelpark Arenberg 10, B-3001, Leuven, Belgium

§ - KU Leuven, Department of Chemistry, Celestijnenlaan 200G-F, B-3001 Heverlee, Belgium

¦ - Hasselt University, Institute for Materials Research & IMEC-associated lab IMOMEC, Wetenschapspark 1, B-3590 Diepenbeek, Belgium

Keywords: Fullerenes, Oxygen, Organic Solar Cells, Stability, Degradation

Abstract: Fullerene based molecules are the archetypical electron accepting materials for organic photovoltaic devices. A detailed knowledge of the degradation mechanisms that occur in C_{60} layers

will aid in the development of more stable organic solar cells. Here, the impact of storage in air on the optical and electrical properties of C_{60} is studied in thin films and in devices. Atmospheric exposure induces oxygen trap states that are 0.19 eV below the LUMO of the fullerene C_{60}. Moreover, oxygen causes a 4-fold decrease of the exciton lifetime in C_{60} layers, resulting in a 40% drop of short-circuit current from optimized planar heterojunction solar cells. The presence of oxygen trap states increases the saturation current of the device, resulting in a 20% loss of open-circuit voltage. Design guidelines are outlined to improve air stability for fullerene-containing devices.

1. Introduction

Fullerene C_{60} was one of the first discovered organic n-type materials and has since been implemented in a multitude of organic semiconductor devices. Field-effect transistors based on C_{60} layers show relatively high on-off ratios (> 10^6) and high charge carrier mobilities (3 $cm^2\ V^{-1}\ s^{-1}$).[1] Notably, fullerenes are most commonly employed in the field of organic photovoltaics, being the archetypical acceptor material in organic solar cells. They are employed either as- is or with additional functional groups that increase their solubility.[2]

Despite being extensively used, C_{60} is known to degrade by several stress factors. For instance, C_{60} degrades under UV light[3,4] and its consequences at the device level were recently modeled for planar heterojunctions solar cells.[5] Similarly, the reduction of carrier mobility[6–9] and conductivity[10–13] upon oxygen exposure of C_{60} layers has been reported. However, neither modeling nor quantification of this oxygen-induced degradation in organic solar cells has been described.

In this work, we investigate how oxygen-induced degradation of C_{60} impacts organic solar cells. We first study the optical changes of C_{60} films exposed to oxygen. Time-resolved

photoluminescence (PL) of C_{60} films shows that oxygen causes a 4-fold decrease of the weighted exciton lifetime. Subsequently, we focus on the air degradation of a prototypical small molecule phthalocyanine (ZnPc) / C_{60} based planar heterojunction device. We compare the degradation of two device stacks in atmospheres with different relative humidity (RH), *i.e.* dry (<0.5% RH) and controlled ambient air (33% RH), and show that oxygen diffusion into the photoactive layers (PAL) is responsible for a 40% short-circuit current density (J_{sc}) decrease. The reduction of the exciton diffusion length, coupled with the increase of the saturation current due to the increase of trap states, results in a 20% decrease of open-circuit voltage (V_{oc}) in 111 h (the time for oxygen to diffuse into C_{60}). We further determine that even in ambient air, in which moisture is present, oxygen is the primary driver of degradation, while moisture accelerates it.

2. Results and Discussion

2.1 Optical Properties of Fullerene C_{60} Films

We first measure the PL lifetime of C_{60} films stored in the dark in either nitrogen, controlled air (33% RH), or dry air (<0.5% RH) to evaluate the role of oxygen and moisture in exciton quenching. The singlet emission at λ=720 nm[14] of 200 nm C_{60} films is measured after excitation with a λ=480 nm laser. The normalized PL of the C_{60} films stored in nitrogen and after 18 h and after 69 h storage in dry air are presented in Figure 1. The exponential decays of the films are fit with either a mono- or double-exponential decay.

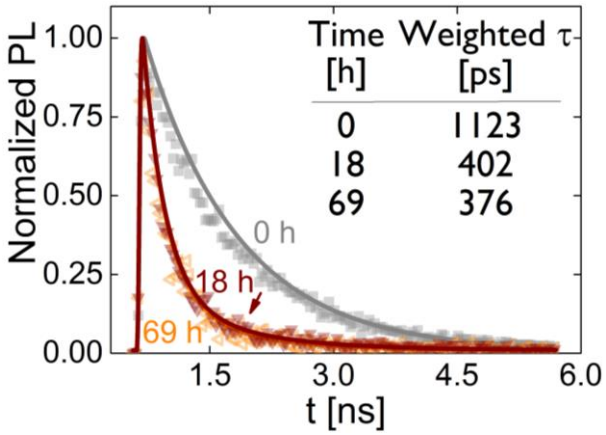


Figure 1. Normalized 720 nm PL emission of 200 nm thick C_{60} films stored in nitrogen (grey squares) and after dry air storage for 18 h (dark red triangles) and for 69 h (open orange triangles). The lines are the exponential fits.

The PL signal of pristine C_{60} films are fit by a mono-exponential decay. From the fit, we calculate the lifetime of the singlet to be 1.12 ns. This value is in agreement with previous reports of singlet lifetime of C_{60} and C_{60} derivatives determined by intersystem crossing and radiative decay and measured both in film and solution.[15–17] The fluorescence decay of dry air stored films are fit by a double-exponential function. In these films, the PL decay contains an additional component, a dominant decay with a lifetime of 267 ± 3 ps (Table S1), resulting in a weighted exciton lifetime of 388 ± 12 ps. This shorter decay cannot be explained by direct oxygen quenching of C_{60} singlets.[18] A decay with similar lifetime (250 ps) was reported by Yang et. al. when studying the PL of C_{60} films over a range of laser fluences.[15] This fast decay occurs at high fluences, hence high exciton concentrations, and is attributed to singlet-singlet annihilation. Increasing singlet-singlet annihilation will reduce the steady state singlet population and, hence, the amount of triplets generated through intersystem crossing. Our fits of oxygen exposed films require this faster decay

component to have a larger contribution than what Yang et. al. report at the highest laser fluence tested (Table S1). Since storage in dry air reduces the PL of C_{60}, compared to pristine C_{60}, the increase of singlet-singlet annihilation cannot be due to an increase of exciton concentration. Therefore, we posit that oxygen in the C_{60} crystals work as a trap sites for excitons (discussed below), enhancing exciton quenching by singlet-singlet annihilation.

Oxygen diffusion into 200 nm C_{60} saturates in less than 18 h, because there is no significant difference in PL beyond this dry air storage time (Figure 1). Hence, oxygen diffusion into thinner C_{60} films, like the 50 nm in the studied devices, is also expected to happen in the same timescale. Furthermore, we determine that water vapor does not have significant influence on the lifetime of C_{60} excitons, because films stored in controlled ambient air and dry air have practically identical exciton lifetimes (Figure S1). The observation that water has no significant effect in C_{60} films is in agreement with density functional theory (DFT) calculations.[19]

2.2 Degradation of Fullerene C_{60} Films in Planar Heterojunctions

In order to understand the impact of oxygen and moisture in shelf-life conditions (under dark and at room temperature), non-encapsulated samples are stored in different atmospheres. Complete stack (CS) samples (Indium Tin Oxide (ITO) / MoO_3 / ZnPc / C_{60} / bathocuproine (BCP) / Ag) are stored in nitrogen, dry air and controlled ambient air and periodically taken from storage for electrical and optical characterization (Figure 2, left). We also store partial stack (PS) samples (ITO / MoO_3 / ZnPc / C_{60}) in dry air before completing and characterizing them (Figure 2, right). Partial stacks permit an easier investigation of the effects of oxygen on the degradation of the PAL without the interference of possible top contact degradation.

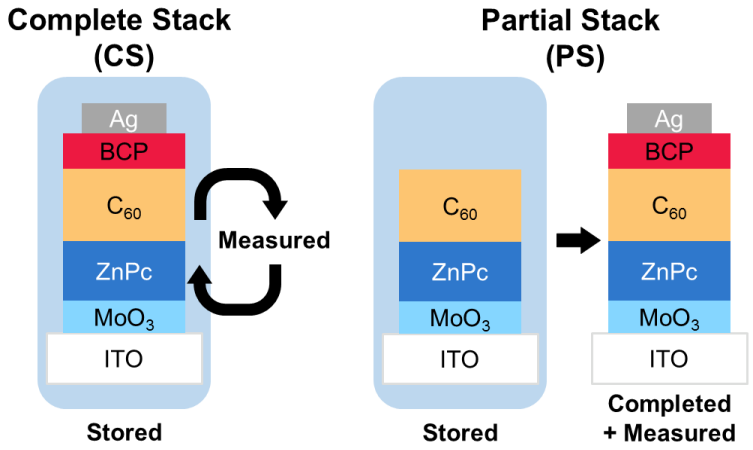


Figure 2. Left: scheme of the complete device stacks (ITO / MoO_3 / ZnPc / C_{60} / BCP / Ag) showing how they are periodically measured and returned to their storage atmosphere. Right: scheme of partial stack (ITO / MoO_3 / ZnPc / C_{60}), which are exposed to the degrading atmosphere, transported to a nitrogen atmosphere, completed with the top contact (BCP / Ag) and measured.

From current density–voltage (*J-V*) measurements, the initial, and final, power conversion efficiency (PCE), J_{sc}, V_{oc}, fill factor (*FF*) and series resistance (R_s obtained through the fitting of dark measurements to the generalized Shockley equation)[20] of the CS samples stored in different atmospheres are summarized in Table 1.

Table 1. PCE, J_{sc}, V_{oc} and *FF* measured under 100 mWcm^{-2} AM1.5G simulated solar illumination and calculated values of R_s at 0 h and 625 h. Values are averages of 6 to 12 devices on one substrate.

	Time [h]	PCE [%]	J_{sc} [mA cm^{-2}]	$J_{sc,EQE}$ [mA cm^{-2}]	V_{oc} [mV]	*FF* [-]	R_s [Ω cm^2]
Nitrogen	0	1.83±0.05	6.5±0.1	6.0	526±5	54.4±0.6	1.8±0.8

Dry Air	625	1.59±0.04	5.7±0.1	-	510±6	55.1±0.5	1.9±0.8
	0	1.78±0.04	6.4±0.1	-	525±5	54.7±0.6	1.8±0.8
	625	0.28±0.01	2.6±0.1	2.3	430±6	25.8±0.5	613.4±40.7
Ambient Air	0	1.81±0.04	6.4±0.1	-	526±7	55.0±0.4	1.6±0.8
	625	0.18±0.01	2.2±0.1	2.3	428±7	20.1±0.4	4276±301.5

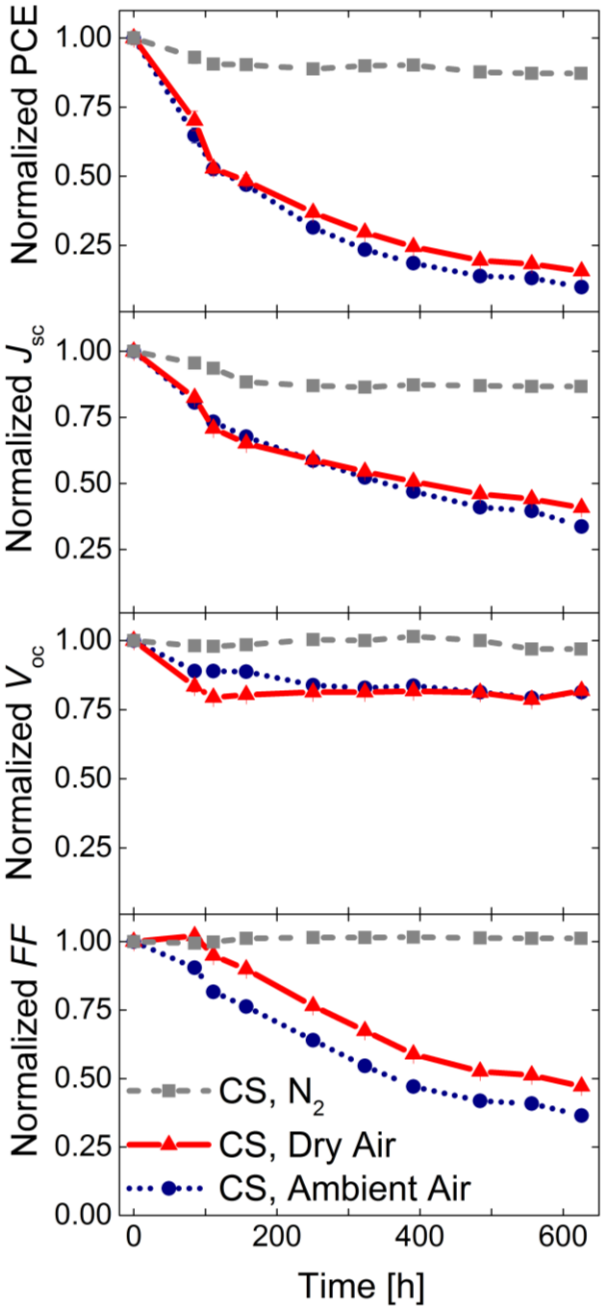


Figure 3. Normalized PCE, J_{sc}, V_{oc} and *FF* extracted from measurements under 100 mW cm^{-2} AM1.5G simulated solar illumination. CS devices were stored in dark and either in N_2 (grey squares with dashed line), dry air (red triangles with continuous line), or ambient air (blue circles with dotted line). The values are averages of 12 devices on one substrate.

2.2.1. Analysis of PCE Loss

The PCE of the CS devices stored in controlled ambient and dry air drop to 10% and 15% of their initial value, respectively, after 625 h (Figure 3). This degradation is driven by the continuous decrease of J_{sc} and *FF*, while V_{oc} stabilizes after an initial decay. Despite the delayed loss of *FF* in devices stored in dry air, the degradation rate of all characteristic parameters is almost identically in the two atmospheres, an indication that oxygen is the main driver for degradation. Moreover, increasing the RH of the storage environment from <0.5% to 33% causes a limited 5% extra loss of PCE over 625 h. These two observations point to oxygen being the dominant stress factor leading to failure in shelf-life conditions. Based on this inference, we focus on understanding the degradation of samples in dry air atmosphere for the remainder of the article.

2.2.2. Origin of J_{sc} Loss

Complete stacks stored in dry air lose 60% of their initial J_{sc} over 625 h. The source of the J_{sc} decrease must lay in at least one of the following steps: (1) absorption of photons by the PAL and generation of excitons; (2) diffusion of excitons to the donor-acceptor interface to form charge-transfer (CT) states; (3) splitting of CT states into charge carriers; (4) collection of charge carriers at the contacts. Since the reflectance of CS stored in air stored remains unaltered after storage in air for 625 h (Figure S2), we can readily exclude changes in the optical properties as the cause of

J_{sc} reduction. The comparison of the external quantum efficiencies (EQE, see Figure 4) of the pristine and dry air stored CS show a substantial signal decrease in the absorption range of C_{60} (peaks at 450 and 500 nm), a faster decrease compared to the one for the signal in the ZnPc absorption range (peaks at 590 and 700 nm). This larger reduction is a strong indication of a material specific loss process, such as reduction of exciton diffusion length (L_D). To investigate this process and other changes in the PAL that can reduce the photocurrent of devices, like increase of trap states due to oxygen intercalation, we focus on PS, which have fresh ETL and contacts.

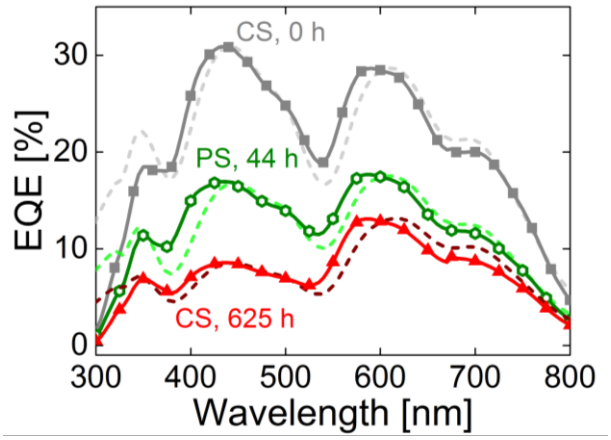


Figure 4. EQE of a pristine CS (closed grey squares) and of a CS after 625 h storage in dry air (closed red triangles). EQE of a PS after 44 h storage in dry air (open green circles). Dashed lines were obtained through simulation using a transfer matrix method.

Partial stacks stored in dry air immediately lose 40% of the J_{sc} and longer storage leads to a further slight reduction of J_{sc}, at a slower rate than what is observed for CS (Figure 5). Hence, in contrast to CS, degradation of PS presents only one slope, or regime. Furthermore, the initial quick loss of J_{sc} in CS happens in the same time frame of V_{oc} loss. Since the V_{oc}, depends only on the state of the PAL (discussed in section 2.2.3), we posit that the initial J_{sc} slope of CS is dominated

by oxygen diffusion through the ETL to the PAL. The second slope is dominated by ETL degradation (discussed below). This also implies that although the diffusion rate of oxygen in BCP is high, the reaction kinetics are lower than in the PAL.

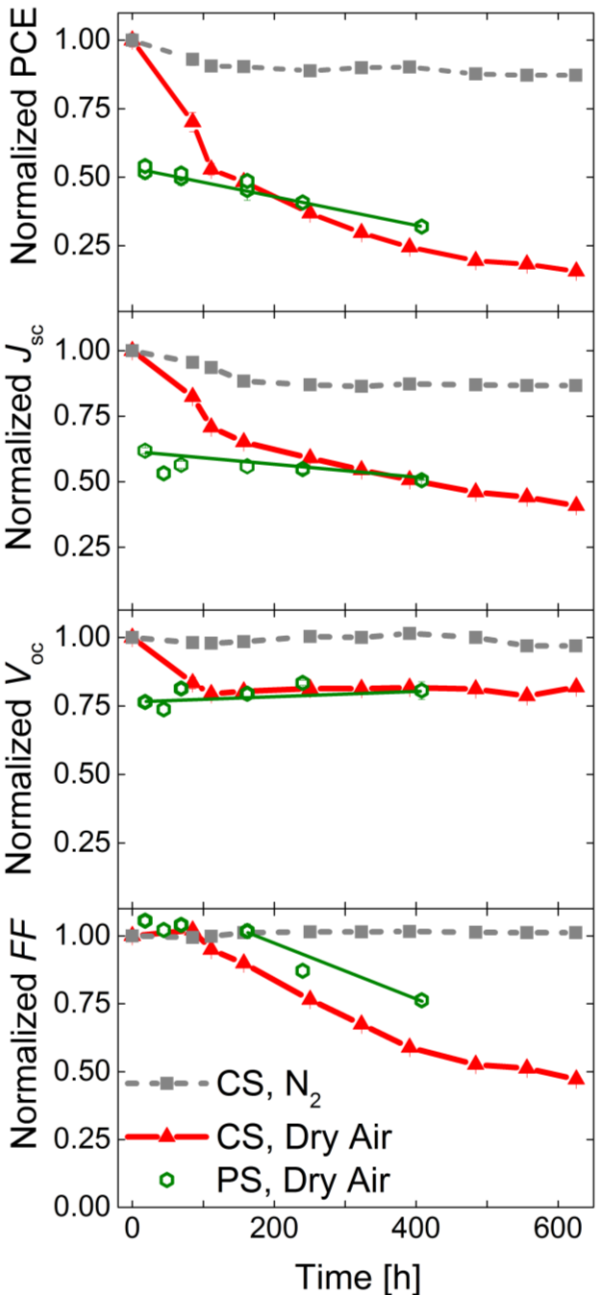


Figure 5. Normalized PCE, J_{sc}, V_{oc} and *FF* of CS and PS devices extracted from measurements under 100 mW cm^{-2} AM1.5G simulated solar illumination. Values given for CS devices stored in dark in either N_2 (grey dotted line and squares) or dry air (red continuous line and triangles) are the same of Figure 3. The values of CS are averages of 12 devices on 1 substrate. The values presented for PS (green open hexagons) are normalized to the initial average values of the two CS samples (PCE = 1.81 ± 0.04%; J_{sc} = 6.4 ± 0.1 mA cm^{-2}; V_{oc} = 526 ± 6 mV, and *FF* = 54.7 ± 0.6%). The lines connect the same CS sample over time while each point of a PS corresponds to a sample.

Comparison of the EQE of pristine CS and PS stored in dry elucidates effect of oxygen on the L_D of the PAL. The EQE of PS stored in dry air shows that the immediate photoresponse loss is due to a more severe reduction of C_{60} signal than that of ZnPc, just like the CS stored for 625 h (Figure 4). To further investigate the uneven decrease of the photo-response we fit the EQE of pristine CS and of PS stored in dry air using a transfer matrix method coupled with a diffusion solver to extract L_D (Figure 4). In this model, we take a perfect charge collection efficiency for both types of devices in the simulations, assuming that oxygen does not affect charge transport severely (discussed below). These fittings reveal the L_D of ZnPc decreases from 12.0±1 nm to 7.0±1 nm while the L_D in C_{60} decreases from 25.0±1 nm to 14.5±1 nm, respectively.

The ratio of the L_D of C_{60} before and after oxygen quenching can also be estimated using the PL lifetimes of the films. Assuming the exciton diffusion coefficient, *D*, is an intrinsic material property that is not affected by exciton quenching defects (oxygen),[21] the ratio between the initial and final L_D is given by:

$$\frac{L_{D_i}}{L_{D_f}} = \frac{\sqrt{D \cdot \tau_i}}{\sqrt{D \cdot \tau}} = \frac{\sqrt{\tau_i}}{\sqrt{\tau}} = \sqrt{\frac{1123}{388}} = 1.70 \quad (1)$$

where τ_i is the exciton lifetime in pristine C_{60} films and τ is the exciton lifetime of C_{60} films after oxygen exposure. The calculated ratio is in agreement with the ratio obtained from the EQE measurements (1.72). The match shows that oxygen molecules in C_{60} films effectively quench excitons, thereby reducing the L_D. The triplet excitons population that are generated via intersystem crossing are determined by the lifetime of the singlet excitons, hence the same lifetime ratio as presented in Eq 1 can be used. Oxygen quenching of singlet excitons reduces the J_{sc} contribution of the C_{60} layer by 42%. Furthermore, the EQE of PS stored for even longer times is unaltered (Figure S3), again showing there is a limit to the oxygen uptake of the PAL. Hence, the maximal concentration of oxygen in the PAL induces a decrease in exciton population that results in an overall J_{sc} decrease of 40%.

The following step in the generation of free charge carriers is the dissociation of the CT states into charge carriers. Exciton dissociation occurs at the donor/acceptor interface, where the HOMO-LUMO energy offsets can overcome the coulombic forces binding the charges carriers. The efficiency of CT state dissociation should not be affected by oxygen since the morphology and the PAL materials should not be altered by oxygen. Oxygen atoms at the interface might induce trap states that increase the CT recombination. These trap states are discussed below.

Next, we examine the effect of oxygen on charge transport in the PAL, which impacts charge collection at the contacts. Charge transport in the PAL can be hindered by the introduction or increase of traps, that decrease the mobility or increase the recombination current. The concentration of exciton quenching sites in small molecules and polymers, was shown to be nearly identical to the concentration of traps, and posited to have the same nature.[21] We have already determined the existence of exciton quenching sites and therefore investigate the formation of carrier traps states upon storage of our devices in dry air. Impedance spectroscopy has been proved

to be effective in the detection of trap states in thin film planar heterojunctions.[22] We measure the CV response of pristine CS, and of CS and PS stored in dry air for 69 h. By analysis of frequency (10^2 to 10^6 Hz), temperature (168 K to 248 K) and bias (–1 to 0.5 V) dependent capacitance measurements we identify a trap signature in PS devices stored in dry air (Figure 6). We calculate an activation energy of 0.19 eV for the identified trap states. This activation energy closely matches the value of previous reports of oxygen-induced traps in C_{60}.[8,9] The claim is further grounded on DFT calculations for the energy of oxygen traps in octahedral voids of C_{60} crystals.[19] The CS stored in dry air present trap features similar to the PS but with lower intensity and no trap features are identified from the CV response of pristine CS (Figure S4). This is explained by C_{60} being directly exposed to oxygen in PS, readily creating traps, while for CS oxygen needs to diffuse through BCP/Ag to reach C_{60}, leading to a lower trap response after the same storage time.

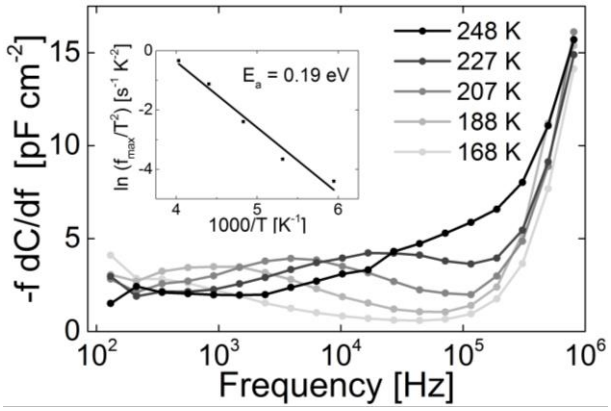


Figure 6. Admittance spectra derived from the capacitance data for different temperatures. Inset shows the Arrhenius plot of the frequency corresponding to the maximum in the admittance peak.

We estimate the trap concentration assuming it is identical to the concentration of exciton quenching defects,[21] that we calculate using through the Stern-Volmer equation:

$$\frac{1}{\tau} = \frac{1}{\tau_i} + 4\pi r D c \qquad (2)$$

where τ is the exciton lifetime of the film exposed to oxygen; τ_i the intrinsic exciton lifetime measured in a diluted C_{60} solution (1.2 ns);[14] r the exciton radii, typically taken as the distance between two C_{60} centers, 1 nm;[23,24] D the exciton diffusion coefficient, calculated from the extracted exciton diffusion length and exciton lifetime to be 5.2 x 10^{-3} cm^2 s^{-1}, in line with values calculated for other organic molecules;[21] and c the concentration of exciton quenching defects. Using this equation, the concentration of exciton quenching defects in C_{60} stored in dry air is 2.66 x 10^{17} cm^{-3}, similar to the concentration reported for other organic small molecules and polymers.[21] Taking this concentration to be identical to the active trap concentration and knowing the molecular density of C_{60} (1.44 x 10^{21} cm^{-3})[25] we reach a C_{60} to oxygen-induced trap ratio of 5404:1. We note that this is a rough estimate since the Stern-Volmer formula is only adequate for materials that present a mono-exponential PL decay with and without traps states. We can compare the calculated value with the surface trap concentration measured by Matsushima et. al in C_{60} transistors after exposure to air.[9] Assuming that trap states correspond to oxygens in octahedral voids[19] of a C_{60} [100] plane (the FCC lattice constant is 1.4 nm), the C_{60} to oxygen-induced trap ratio is 9578:1, which is of the same order of magnitude of the value we calculated.

Oxygen creates shallow traps, therefore charge trapping and de-trapping can happen, decreasing charge mobility, and increasing the R_s. Indeed, oxygen exposure of C_{60} films was shown to decrease charge carrier mobility.[7–9,13,25] Contrarily, ZnPc is doped by oxygen, albeit inefficiently,[26] increasing its conductivity.[27–29] As a result, we expect the PAL conductivity to decrease, causing an overall increase of R_s. To probe this assumption we compare R_s of PS stored in dry air and pristine CS. The fitting of the dark *J-V* characteristics shows the R_s of PS stored in dry air is only slightly higher than that of pristine CS (Table 2), indicating that oxygen exposure of the PAL does not cause a significant change to the resistance of the full device. This is translated in an unaffected

FF comparing degraded PS and pristine CS, despite the large difference in J_{sc} (Figure 5). Therefore, our data clearly demonstrates that oxygen does not affect the resistivity of the PAL in a significant way and is not an important source of J_{sc} loss.

Table 2. J_{sc}, J_0, n, R_s $V_{oc,calculated}$ and $V_{oc,measured}$ of a pristine complete stack device and a partial stack device after 18 h in dry air. The J_{sc} and $V_{oc,measured}$ are measured in a solar simulator under 100 mW cm^{-2} AM1.5 conditions. J_0 and n were obtained by fitting the dark curve of the devices with a Shockley equation. $V_{oc,calculated}$ was calculated based on the values extracted with the generalized Shockley equation.

Type of device	Time in Dry Air	J_{sc}	J_0	n	R_s	$V_{oc,calculated}$	$V_{oc,measured}$
	[h]	[mA·cm^{-2}]	[μA·cm^{-2}]	[ ]	[Ω·cm^2]	[mV]	[mV]
Complete	0	6.4±0.1	50.5±6.3	1.9±0.1	1.9±0.9	561	538±5
Partial	18	4.1±0.1	350.0±59.6	1.8±0.1	2.7±0.9	437	407±7

The increase of trap concentration can also increase recombination, although shallow traps are inefficient recombination centers. We analyze the ideality factor (n) to probe if recombination is important in the operation of the devices. The n extracted from the fit of the dark *J-V* characteristics of pristine CS is 1.9 while that of PS stored in dry air is 1.8 (Table 2). These values indicate 'Shockley-Read-Hall'-like recombination in the device, independent of the presence of oxygen in the PAL.[20] This observation is in line with the previous reports of a trap state 0.42 eV below C_{60}'s LUMO, which is independent of oxygen concentration in C_{60} films.[9] Although we could not identify this deep trap state, as it falls outside the range of our CV set-up, we believe it is the cause of the high measured n. This deeper trap state will drive recombination more substantially compared to the shallow one identified above. Regardless, any new trap state in the bandgap should

contribute to an increase of the saturation current density (J_0), as additional traps reduce the energy required for band to band excitation. The J_0 derived from fitting the dark *J-V* characteristics of pristine CS is seven times larger than that of dry air stored PS (Table 2). This value does not represent a significant increase, in line with what is expected for a rather shallow trap like the one identified. Thus in our view, this indicates that the shallow traps created by oxygen do not alter the recombination process severely to influence the device characteristics. However, the possibility that oxygen induces traps in other layers, increasing recombination and decreasing charge collection, is not excluded.

Finally, the collection of charges is affected by the condition of the contacts. Losses at the contacts are inferred from the comparison of the CS and PS stored in dry air. The CS stored in dry air lose J_{sc} at a higher rate than PS, exceeding the total J_{sc} loss of PS after 408 h. Hence, the larger J_{sc} reduction of CS can only be explained by additional degradation of the ETL or C_{60}/ETL. Exciton-polaron annihilation at the C_{60}/BCP was identified in devices identical to those here investigated[30] and shown to reduce J_{sc} of pristine devices by 15%.[31,32] To determine whether this process is enhanced by oxygen we fit the slope of reverse bias region the of the *J-V* characteristics of pristine CS, CS stored in nitrogen, and in dry air, and of PS stored in dry air (Figure S5). We determine the slope of the reverse bias region to be approximately the same for all devices (1 mA/V), showing exciton-polaron annihilation does not increase due to oxygen and posit that the C_{60}/BCP interface is not affected. Therefore the source of J_{sc} charge loss should lay in the ETL.

The 60% J_{sc} loss in CS over the 625 h of dry air storage is accompanied by an R_s increase of two orders of magnitude (Table 1). We note this value is an overestimation since devices stored in dry air present photoconductivity (Figure S6), and we fit the device in the dark. Also, the PS do not display s-shaped *J-V* characteristics like CS, even after storage times longer than 390 h (Figure

S7). Therefore, the degraded ETL should be the source of the increased R_s. An additional extraction barrier due to the degraded ETL promotes recombination, decreasing charge carrier collection. This hypothesis aligns with recent reports of Hao et al., who observed an increase of trap recombination after storing devices similar to ours in air.[33] Moreover, there are several reports of BCP degradation in air.[34–37] Thus, the increase in extraction barriers is responsible for the remaining 20% J_{sc} reduction observed in CS.

In summary, the quenching of excitons by oxygen accounts for 40% relative loss of the J_{sc}, while extraction barriers account for the extra 20% loss (Figure 7).

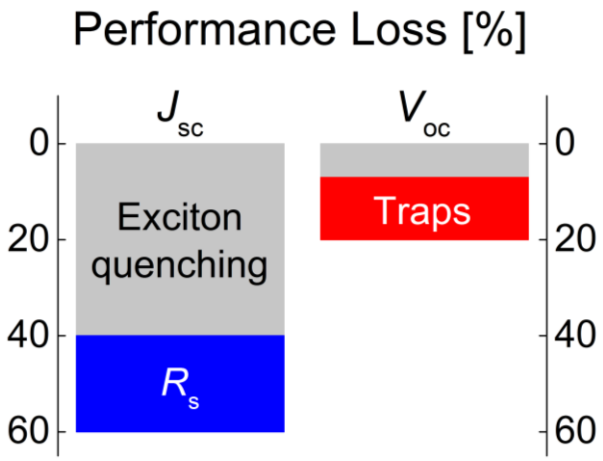


Figure 7. Summary of the J_{sc} and V_{oc} loss, the source of the loss for CS devices stored during 625 h in dry air.

2.2.3. Origin of V_{oc} Loss

After 111 h of storage in dry air, the V_{oc} of CS and PS stabilized at approximately 80% of the initial V_{oc} values. For PS, the decrease in V_{oc} is immediate, coinciding with that observed for J_{sc}. For CS, the V_{oc} decreases progressively until it stabilizes after 111 h. The V_{oc} stabilization is

independent of the atmosphere, hole transport layers (Figure S8) and of the degree of atmospheric exposure of the ETL (CS vs PS), which indicates that the V_{oc} reduction is solely due to the effect of oxygen in the PAL. To understand the origin of the V_{oc} loss we investigate whether oxygen changes the energy of the charge transfer state (E_{CT}). The V_{oc} is known to depend linearly on E_{CT}[38–40] and can be measured by Fourier transformed photo-response spectroscopy (FTPS). Our measurements show that there is no change of E_{CT} upon oxygen diffusion into the PAL (1.09 eV for pristine CS vs 1.08 eV for dry-air exposed PS, Figure S9). The unchanged E_{CT} is in agreement with the literature, because it depends on the donor-acceptor pair and their ratio, and no change of composition or significant chemical changes are expected in dry air.[4,27,28,41] Thus, the drop in V_{oc} can only be related to the decrease in the generated charge carriers and the increase in saturation current upon oxygen exposure. Based on this assumption we calculate V_{oc} according to the following equation:

$$V_{OC} = \frac{nkT}{q} \ln\left(\frac{J_{sc}}{J_0} + 1\right) \qquad (3)$$

where n is the ideality factor, k the Boltzmann constant, T the temperature, q the elementary charge and J_0 the saturation current. The calculated V_{oc} are 20-30 mV in excess of the measured values but in agreement with them. According to these calculations the decrease of J_{sc} accounts for 34 mV of loss in V_{oc} (6% reduction in relation to the initial value) while the remaining 90 mV loss (16% reduction in relation to the initial value) is due to the increase of the saturation current that we correlated above with the formation of traps (Figure 7).

3. Conclusion

We investigated the effect of oxygen degradation of C_{60} films in both thin films and devices. We correlated the PL changes of C_{60} films stored in oxygen with the degradation mechanisms of a

prototypical small molecule solar cell in ambient air and observed that oxygen is responsible for the majority of the J_{sc} loss by promoting exciton quenching. The degradation of the ETL and/or C_{60}/ETL plays a secondary role. The reduction of V_{oc} is due to an increase of saturation current in combination with a decrease of generated charges due to exciton quenching. Thus oxygen is identified as the main source of degradation, while moisture has an accelerating factor.

The identified degradation mechanisms are material (C_{60}) dependent and not related to processing or the device stack. In order to increase the air stability of small molecule devices that make use of C_{60} we should address all the identified mechanisms. According to our results the path to more stable devices would be to increase C_{60} crystallinity, which reduces oxygen diffusion[4,25] use of bulk heterojunction tailored to quickly dissociate excitons and use of the air stable transport layers.[33] Moreover, we demonstrate that the selection of suitable encapsulation should consider oxygen transmission rates, not only the water transmission rates often cited.

4. Experimental Procedures

Materials: Patterned Indium Tin Oxide (ITO) substrates were bought from Colorado Concept. The organic materials fullerene (C_{60}, Nano-C), Zinc Phthalocyanine (ZnPc, Aldrich), BF-DPB (Lumtec), and bathocuproine (BCP, Aldrich) were purified once using gradient sublimation, while silver (Ag, K. J. Lesker), molybdenum tri-oxide (MoO_3, Aldrich), $C_{60}F_{48}$ (Nano-C), and Magnesium Chloride ($MgCl_2$, Aldrich) were used as received.

Device Fabrication and Characterization: Quartz substrates for Photoluminescence (PL) measurements and patterned Indium Tin Oxide (ITO) substrates for Organic Photovoltaic (OPV) devices were cleaned sequentially by sonication with detergent, deionized water, acetone and isopropanol and finally treated with oxygen plasma for 5 minutes. The clean substrates were loaded

to a high vacuum chamber (K.J. Lesker, base pressure, 10^{-6} torr) where the layers were evaporated at a 1 Å/s rate at room temperature.

Fullerene films with a thickness of 50 and 200 nm were deposited on quartz. OPV devices were produced in either 1 (CS) or 2 (PS) steps. The layer structure of the complete stack is the following: (ITO) / MoO_3 (5 nm) / ZnPc (40 nm) / C_{60} (50 nm) / BCP (10 nm) / Ag (120 nm). Partial stack samples were produced with an identical layer configuration as the complete stack until C_{60}. Then this structure was degraded for a pre-determined time and finally loaded in the vacuum chamber for deposition of BCP (10 nm) and Ag (120 nm). In both types of samples the top metal electrode was evaporated through a mask that defined 12 identical cells with an active area of 0.013 cm^2.

Current-voltage characterization was performed in a nitrogen glovebox (water and oxygen levels below 0.1% ppm) with a four probe measurement set-up and an Abet solar simulator (simulated AM1.5G emission) equipped with a KG3 bandpass filter and calibrated to 100 mW cm^{-2} with a certified Fraunhofer cell. The spectral response of the cells was measured using a modified commercial set-up from Bentham. Monochromated, chopped light at a 333 Hz originating from a Xenon arc lamp (300-670 nm) and a quartz halogen lamp (670-900 nm) coupled into the cell, and a lock-in technique were used to determine the external quantum efficiency. Series Resistance was calculated by fitting dark curves to a generalized diode equation while exciton diffusion length was extracted from EQE with a matlab script based on transfer matrix method.

Degradation Conditions and Annealing: Devices and films were aged in controlled environments in the dark at a constant temperature of 20 °C. A controlled ambient atmosphere with 33% RH was created by a supersaturated $MgCl_2$ solution in a sealed container. Dry air (<0.5% RH) was provided by a desiccant dry cabinet.

Time-correlated Single Photon Counting: The fluorescence decay times were determined by T-CSPC using the setup that has been described in detail previously.[42] A time-correlated Single Photon Timing PC module (SPC 830, Becker & Hickl) was used to obtain the fluorescence decay histogram in 4,096 channels. The decays were recorded with 5000 counts in the peak channel, in time windows of 15 ns corresponding to 3.7 ps/channel and analyzed globally as a sum of exponentials with time-resolved fluorescence analysis software.[43] The full width at half-maximum of the IRF was typically in the order of 40 ps. The quality of the fits was judged by the fit parameters χ^2 (< 1.2), $Z\chi^2$ (< 3) and the Durbin Watson parameter (1.8<DW<2.2) as well as by the visual inspection of the residuals and autocorrelation function. Measurements were performed on films with an optical path length of 50 nm and 200 nm at the excitation wavelength of 488 nm.

C-V measurements: Admittance spectroscopy measurements were performed with an Agilent E4980A Precision LCR Meter using a measurement frequency varying logarithmically from 100 Hz to 1 MHz.

FTPS measurements: Fourier Transform Photocurrent Spectroscopy was performed using a Thermo Nicolet 8700 FTIR with an external detector. The spectra were recorded with a quartz beamsplitter and appropriate optical bandpass filters to improve the signal to noise ratio. All spectra were corrected for the frequency response.[44]

ASSOCIATED CONTENT

Supporting Information

Table with the fitting parameters of PL of C_{60} films stored in nitrogen and after storage in dry air; plot of the photoluminescence decay of C_{60} films stored in controlled air and dry air; reflectance of CS, pristine vs after storage in controlled ambient air; admittance spectra derived

from the capacitance data for different temperatures of pristine CS and dry air stored partial stack; EQE of PS after storage for 44 h and 162 h in dry air; *J-V* characteristics of PS and CS; fits of the slopes of the *J-V* characteristics of in reverse bias; Dark and light characteristics of pristine CS, CS stored in nitrogen and in dry air, and of PS stored in dry air; *J-V* characteristics of PS and CS stored in dry air measured under solar illumination; V_{oc} of CS with different transport layers in dry air and controlled air; FTPS measurements of pristine CS and air dry stored PS; J_{sc} of CS Planar heterojunctions and bulk heterojunctions store in nitrogen and in dry air. This material is available free of charge via the Internet at http://pubs.acs.org.

AUTHOR INFORMATION

Corresponding Author

* Joao Bastos – joao.bastos@imec.be

Author Contributions

The manuscript was written through contributions of all authors. All authors have given approval to the final version of the manuscript.

Funding Sources

The research leading to these results has received funding from the European Community's Seventh Framework Program (FP7/2007-2013) under Grant Agreement 287818 of the X10D project.

ACKNOWLEDGMENT

The authors wish to thank: Erwin Vandenplas, for processing support and sample preparation; Jeffrey Tait, for reviewing the paper and Dr. Gehlhaar for the fruitful discussions.

ABBREVIATIONS

ZnPc, zinc phthalocyanine

RH, relative humidity

J_{sc} , short circuit current density

V_{oc}, open circuit voltage

RH, relative humidity

DFT, density functional theory

ITO, indium tin oxide

MoO_3, molybdenum oxide

BCP, bathocuproine

Ag, silver

PCE, power conversion efficiency

FF, fill factor

R_s, series resistance

PAL, photo-active layer

J-V, current density-voltage

PS, partial stack device

CS, complete stack device

EQE, external quantum efficiency

CV, capacity voltage

LUMO, lowest occupied molecular orbital

J_0, saturation current density

n, ideality factor

E_{CT}, charge transfer

FTPS, Fourier Transformed Photo-response Spectroscopy

D, exciton diffusion coefficient

L_D, exciton diffusion length

ETL, electron transport layer

HTL, hole transport layer

REFERENCES

(1) Kitamura, M.; Aomori, S.; Na, J. H.; Arakawa, Y. Bottom-Contact Fullerene C60 Thin-Film Transistors with High Field-Effect Mobilities. *Appl. Phys. Lett.* **2008**, *93* (3), 033313.

(2) Voroshazi, E.; Vasseur, K.; Aernouts, T.; Heremans, P.; Baumann, A.; Deibel, C.; Xue, X.; Herring, A. J.; Athans, A. J.; Lada, T. a.; Richter, H.; Rand, B. P. Novel Bis-C60 Derivative Compared to Other Fullerene Bis-Adducts in High Efficiency Polymer Photovoltaic Cells. *J. Mater. Chem.* **2011**, *21* (43), 17345.

(3) Juha, L.; Kr, J.; Lfiska, L.; Hamplovfi, V.; Soukup, L.; Engst, P.; Kubfit, P. Fast Degradation of Fullerenes by Ultraviolet Laser Radiation. *Appl. Phys. B* **1993**, *84* (57), 83–84.

(4) Makarova, T.; Sakharov, V. Light-Induced Transformation of C60 Films in the Presence and Absence of Oxygen. *Phys. Solid State* **1999**, *41* (3), 3–6.

(5) Burlingame, Q.; Tong, X.; Hankett, J.; Slootsky, M.; Chen, Z.; Forrest, S. R. Photochemical Origins of Burn-in Degradation in Small Molecular Weight Organic Photovoltaic Cells. *Energy Environ. Sci.* **2015**, *8* (3), 1005–1010.

(6) Arai, T.; Murakami, Y.; Suematsu, H.; Kikuchi, K.; Achiba, Y.; Ikemoto, I. Resistivity of Single Crystal C60 and Effect of Oxygen. *Solid State Commun.* **1992**, *84* (8), 827–829.

(7) Tapponnier, A.; Biaggio, I.; Günter, P. Ultrapure C60 Field-Effect Transistors and the Effects of Oxygen Exposure. *Appl. Phys. Lett.* **2005**, *86* (11), 112114.

(8) Habuchi, H.; Nitta, S.; Han, D.; Nonomura, S. Localized Electronic States Related to O2 Intercalation and Photoirradiation on C60 Films and C70 Films. *J. Appl. Phys.* **2000**, *87*

(12), 8580.

(9) Matsushima, T.; Yahiro, M.; Adachi, C. Estimation of Electron Traps in Carbon-60 Field-Effect Transistors by a Thermally Stimulated Current Technique. *Appl. Phys. Lett.* **2007**, *91* (10), 103505.

(10) Hamed, A.; Sun, Y. Y.; Tao, Y. K.; Meng, R. L.; Hor, P. H. Effects of Oxygen and Illumination on the in Situ Conductivity of C60 Thin Films. *Phys. Rev. B* **1993**, *47* (16), 10873–10880.

(11) Moses, D.; Lee, C.; Kraabel, B.; Yu, G.; Srdanov, V. Photocarrier Dynamics in C60: Studies of Transient Photoconductivity and Transient Photoinduced Absorption. *Synth. Met.* **1995**, *70* (1-3), 1419–1422.

(12) Lee, C. H.; Yu, G.; Kraabel, B.; Moses, D.; Srdanov, V. I. Effects of Oxygen on the Photocarrier Dynamics in a Dynamics in a C60 Film: Studies of Transient and Steady-State Photoconductivitity. *Phys. Rev. B* **1994**, *49* (15), 10572–10576.

(13) Könenkamp, R.; Priebe, G.; Pietzak, B. Carrier Mobilities and Influence of Oxygen in C60 Films. *Phys. Rev. B* **1999**, *60* (16), 804–808.

(14) Ebbesen, T. W.; Tanigaki, K.; Kuroshima, S. Excited-State Properties of C60. *Chem. Phys. Lett.* **1991**, *181* (6), 501–504.

(15) Yang, S. I.; Suh, Y. D.; Jin, S. M.; Kim, S. K.; Park, J.; Shin, E.; Kim, D. Energy Relaxation Dynamics of Photoexcited C 60 Solid. *J. Phys. Chem.* **1996**, *100* (22), 9223–9226.

(16) Lee, M.; Song, O.-K.; Seo, J.-C.; Kim, D.; Suh, Y. D.; Jin, S. M.; Kim, S. K. Low-Lying Electronically Excited States of C60 and C70 and Measurement of Their Picosecond Transient Absorption in Solution. *Chem. Phys. Lett.* **1992**, *196* (3-4), 325–329.

(17) Van Duren, J. K. J.; Yang, X.; Loos, J.; Bulle-Lieuwma, C. W. T.; Sieval, A. B.; Hummelen, J. C.; Janssen, R. A. J. Relating the Morphology of Poly(p-Phenylene Vinylene)/ Methanofullerene Blends to Solar-Cell Performance. *Adv. Funct. Mater.* **2004**, *14* (5), 425–434.

(18) Arbogast, J. W.; Darmanyan, A. P.; Foote, C. S.; Diederich, F. N.; Whetten, R. L.; Rubin, Y.; Alvarez, M. M.; Anz, S. J. Photophysical Properties of Sixty Atom Carbon Molecule (C60). *J. Phys. Chem.* **1991**, *95* (1), 11–12.

(19) Tsetseris, L.; Pantelides, S. T. Oxygen and Water-Related Impurities in C60 Crystals: A Density-Functional Theory Study. *Phys. Rev. B* **2010**, *82* (4), 045201.

(20) Cheyns, D.; Poortmans, J.; Heremans, P.; Deibel, C.; Verlaak, S.; Rand, B. P.; Genoe, J. Analytical Model for the Open-Circuit Voltage and Its Associated Resistance in Organic Planar Heterojunction Solar Cells. *Phys. Rev. B* **2008**, *77* (16), 165332.

(21) Mikhnenko, O. V; Kuik, M.; Lin, J.; van der Kaap, N.; Nguyen, T.-Q.; Blom, P. W. M. Trap-Limited Exciton Diffusion in Organic Semiconductors. *Adv. Mater.* **2014**, *26* (12), 1912–1917.

(22) Walter, T.; Herberholz, R.; Müller, C.; Schock, H. W. Determination of Defect Distributions from Admittance Measurements and Application to Cu(In,Ga)Se2 Based Heterojunctions. *J. Appl. Phys.* **1996**, *80* (8), 4411–4420.

(23) Cook, S.; Furube, A.; Katoh, R.; Han, L. Estimate of Singlet Diffusion Lengths in PCBM

Films by Time-Resolved Emission Studies. *Chem. Phys. Lett.* **2009**, *478* (1-3), 33–36.

(24) Krätschmer, W.; Lamb, L. D.; Fostiropoulos, K.; Huffman, D. R. Solid C60: A New Form of Carbon. *Nature*. September 27, 1990, pp 354–358.

(25) Pevzner, B.; Hebard, A.; Dresselhaus, M. Role of Molecular Oxygen and Other Impurities in the Electrical Transportand Dielectric Properties of C 60 Films. *Phys. Rev. B* **1997**, *55* (24), 10–15.

(26) van Faassen, E.; Kerp, H. Explanation of the Low Oxygen Sensitivity of Thin Film Phthalocyanine Gas Sensors. *Sensors Actuators B Chem.* **2003**, *88* (3), 329–333.

(27) Collins, R.; Mohammed, K. Electrical, Structural and Gas Sensing Properties of Zinc Phthalocyanine Thin Films. *Thin Solid Films* **1986**, *145* (1), 133–145.

(28) Kerp, H. R.; Westerduin, K. T.; van Veen, A. T.; van Faassen, E. E. Quantification and Effects of Molecular Oxygen and Water in Zinc Phthalocyanine Layers. *J. Mater. Res.* **2001**, *16* (02), 503–511.

(29) Kerp, H. R.; Westerduin, K. T.; van Veen, A. T.; van Faassen, E. E. Quantification and Effects of Molecular Oxygen and Water in Zinc Phthalocyanine Layers. *J. Mater. Res.* **2001**, *16* (02), 503–511.

(30) Verreet, B.; Malinowski, P. E.; Niesen, B.; Cheyns, D.; Heremans, P.; Stesmans, A.; Rand, B. P. Improved Cathode Buffer Layer to Decrease Exciton Recombination in Organic Planar Heterojunction Solar Cells. *Appl. Phys. Lett.* **2013**, *102* (4), 043301.

(31) Jeong, W. I.; Lee, Y. E.; Shim, H. S.; Kim, T. M.; Kim, S. Y.; Kim, J. J. Photoconductivity of C60 as an Origin of Bias-Dependent Photocurrent in Organic Photovoltaics. *Adv. Funct. Mater.* **2012**, *22* (14), 3089–3094.

(32) Renshaw, C. K.; Zimmerman, J. D.; Lassiter, B. E.; Forrest, S. R. Photoconductivity in Donor-Acceptor Heterojunction Organic Photovoltaics. *Phys. Rev. B* **2012**, *86* (8), 085324.

(33) Hao, X.; Wang, S.; Sakurai, T.; Masuda, S.; Akimoto, K. Improvement of Stability for Small Molecule Organic Solar Cells by Suppressing the Trap Mediated Recombination. *ACS Appl. Mater. Interfaces* **2015**, No. 7, 18379–18386.

(34) Wu, H. R.; Song, Q. L.; Wang, M. L.; Li, F. Y.; Yang, H.; Wu, Y.; Huang, C. H.; Ding, X. M.; Hou, X. Y. Stable Small-Molecule Organic Solar Cells with 1,3,5-tris(2-N-Phenylbenzimidazolyl) Benzene as an Organic Buffer. *Thin Solid Films* **2007**, *515* (20-21), 8050–8053.

(35) Song, Q. L.; Li, F. Y.; Yang, H.; Wu, H. R.; Wang, X. Z.; Zhou, W.; Zhao, J. M.; Ding, X. M.; Huang, C. H.; Hou, X. Y. Small-Molecule Organic Solar Cells with Improved Stability. *Chem. Phys. Lett.* **2005**, *416* (1-3), 42–46.

(36) Lare, Y.; Kouskoussa, B.; Benchouk, K.; Ouro Djobo, S.; Cattin, L.; Morsli, M.; Diaz, F. R.; Gacitua, M.; Abachi, T.; del Valle, M. a.; Armijo, F.; East, G. a.; Bernède, J. C. Influence of the Exciton Blocking Layer on the Stability of Layered Organic Solar Cells. *J. Phys. Chem. Solids* **2011**, *72* (2), 97–103.

(37) Yang, Q. D.; Ng, T.-W.; Lo, M.-F.; Wang, F. Y.; Wong, N. B.; Lee, C.-S. Effect of Water and Oxygen on the Electronic Structure of the Organic Photovoltaic. *J. Phys. Chem. C* **2012**, *116* (20), 10982–10985.

(38) Vandewal, K.; Tvingstedt, K.; Gadisa, A.; Inganäs, O.; Manca, J. V. Relating the Open-Circuit Voltage to Interface Molecular Properties of Donor:acceptor Bulk Heterojunction Solar Cells. *Phys. Rev. B* **2010**, *81* (12), 125204.

(39) Deibel, C.; Strobel, T.; Dyakonov, V. Role of the Charge Transfer State in Organic Donor-Acceptor Solar Cells. *Adv. Mater.* **2010**, *22* (37), 4097–4111.

(40) Veldman, D.; Meskers, S. C. J.; Janssen, R. A. J. The Energy of Charge-Transfer States in Electron Donor-Acceptor Blends: Insight into the Energy Losses in Organic Solar Cells. *Adv. Funct. Mater.* **2009**, *19* (12), 1939–1948.

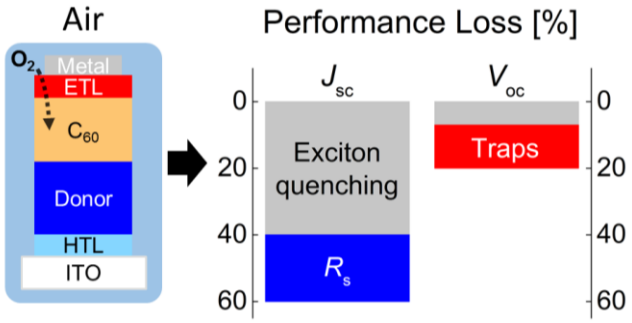
(41) Werner, H.; Schedel-Niedrig, T.; Wohlers, M.; Herein, D.; Herzog, B.; Schlogl, R.; Keil, M.; Bradshaw, A. M.; Kirschner, J. Reaction of Molecular Oxygen with C60: Spectroscopic Studies. *J. Chem. Soc. Faraday Trans.* **1994**, *90* (3), 403.

(42) Maus, M.; Rousseau, E.; Cotlet, M.; Schweitzer, G.; Hofkens, J.; Van der Auweraer, M.; De Schryver, F. C.; Krueger, A. New Picosecond Laser System for Easy Tunability over the Whole Ultraviolet/visible/near Infrared Wavelength Range Based on Flexible Harmonic Generation and Optical Parametric Oscillation. *Rev. Sci. Instrum.* **2001**, *72* (1), 36.

(43) Boens, N.; Qin, W.; Basaric, N.; Hofkens, J.; Ameloot, M.; Pouget, J.; Lefe, J.; Valeur, B.; Gratton, E.; VandeVen, M.; Silva, N. D.; Engelborghs, Y.; Willaert, K.; Sillen, A.; Rumbles, G.; Phillips, D.; Visser, A. J. W. G.; Hoek, A. Van; Lakowicz, J. R.; Malak, H.; Gryczynski, I.; Szabo, A. G.; Krajcarski, D. T. Fluorescence Lifetime Standards for Time and Frequency Domain Fluorescence Spectroscopy. *Anal. Chem.* **2007**, *79* (5), 2137–2149.

(44) Vandewal, K.; Goris, L.; Haeldermans, I.; Nesladek, M.; Haenen, K.; Wagner, P.; Manca, J. V. Fourier-Transform Photocurrent Spectroscopy for a Fast and Highly Sensitive Spectral Characterization of Organic and Hybrid Solar Cells. *Thin Solid Films* **2008**, *516*, 7135–7138.

Table of Contents



Fullerene based molecules are the archetypical electron transport materials for organic photovoltaic devices. However, fullerenes are also very susceptible to degradation. Here the

degradation mechanisms induced by oxygen in C_{60} based devices are identified and their impact in device parameters quantified.